

A Motion Control Scheme for a WMR based on Input-Output Feedback Linearization and PID

Abstract—This paper presents a trajectory tracking control scheme for an underactuated wheeled mobile robot (WMR). The WMR model used includes the robot kinematics and dynamics, as well as some DC motor nonlinearities. A control scheme is proposed contains two loops: the inner one is a PID controller to handle with the dynamics, and the outer one deals with the kinematics, using an input-output feedback linearization of the *Follow the Carrot* approach. Some different shapes of trajectories are devised in order to analyse the feasibility of the method.

I. INTRODUCTION

Three basic control problems can be found in the wheeled mobile robots (WMR) motion control literature: (a) *Point stabilization*: the vehicle is required to stabilize at a given pose (position and heading); (b) *Path following*: the vehicle is required to follow a given geometric path; and (c) *Trajectory tracking*: the vehicle is required to track a trajectory, i.e., a geometric path with temporal properties.

Some control algorithms to solve these problems have been described in the mobile robotics literature [1]. Classical methods, such as the *Follow the Carrot* [2] and the *Pure Pursuit* [3], use robot position information to compute steering commands in order to follow a predefined geometric path. Variations of these algorithms are also found in the literature, see for example, [4] and [5]. These algorithms are known to have poor performance in corners since they do not take into account the actual curvature of the path. Therefore, some complex algorithms have been developed recently.

The *Follow the Past* [6] uses recorded steering commands information to overcome the problem with sharp trajectory tracking found in the classical methods; the *Vector Pursuit* [7], [8] is a geometric path following method based on the screw theory; the *Valued-based controller* [9] integrates the dynamics of the vehicle model in order to predict optimal steering commands; a robust *Model Reference Adaptive Controller* has also been studied for mobile robots with uncertainties in the dynamical model [10].

Encarnaç o and Pascoal [11] introduced a combined trajectory tracking and path following control approach for WMR. This approach has been improved by other researchers [12]–[14].

This paper addresses a trajectory tracking controller for an underactuated WMR complete non-linear model presented by N rgaard et al. [15], using feedback linearization and a typical motion control scheme: the *Follow the Carrot* algorithm.

Even though the feedback linearization approach has been proposed in motion control of WMR [16]–[19], this paper

claims novelty while combining in a dual loop controller, both kinematics feedback linearization under the *Follow the Carrot* approach, and dynamics velocity PID.

The paper is structured as follows. In Section II, a complete model formulation of a WMR is introduced, considering the chassis kinematics/dynamics, and the DC motor non-linear model. The control system scheme is presented in Section III. In Section IV, some simulation results are presented and discussed. Finally, in Section V some conclusions about the feasibility of the proposed control scheme are drawn.

II. THE UNDERACTUATED WMR MODEL

A differential rectangular WMR is made up of a rigid frame equipped by two non deformable motor driven wheels. The robot chassis geometry is defined by the constants: b as the robot width, l its length, r the wheels radii and d_f the distance between the wheels axis and the front of the chassis, as illustrated by the schematic diagram on Figure 1.

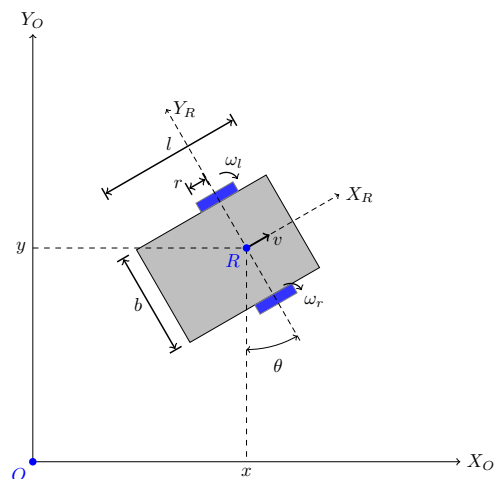


Fig. 1. The differential rectangular WMR and the coordinate frames.

It is assumed that the robot is moving on a horizontal plane with a fixed arbitrary inertial frame $\{O\} = \{X_O, Y_O\}$. The robot coordinate frame $\{X_R, Y_R\}$ is attached to the robot chassis on the reference point given by $R : (x, y)$, which is positioned in the middle of the shaft. The rotation angle between both coordinates frames is given by θ . Therefore, the WMR pose is then completely defined by the vector $\xi_O = [x \ y \ \theta]^T$.

A. Kinematic Model

Since both the wheels are individually controlled, the angular velocities ω_r and ω_l are independents. Their relationship with the robot translation velocity v and with the angular velocity $\dot{\theta}$ can be written as

$$v = r/2(\omega_r + \omega_l), \quad (1)$$

$$\dot{\theta} = r/b(\omega_r - \omega_l). \quad (2)$$

The velocity components of R in the inertial coordinate frame $\{O\}$ are given by $\dot{x} = v \cos\theta$ and $\dot{y} = v \sin\theta$. Hence, the pose time derivative can be presented as the matrix equation

$$\dot{\xi}_O = \begin{bmatrix} \dot{x} \\ \dot{y} \\ \dot{\theta} \end{bmatrix} = \begin{bmatrix} r\cos\theta/2 & r\cos\theta/2 \\ r\sin\theta/2 & r\sin\theta/2 \\ r/b & -r/b \end{bmatrix} \begin{bmatrix} \omega_r \\ \omega_l \end{bmatrix}. \quad (3)$$

Note that the model is underactuated, i.e., the number of independent controls input ($[\omega_r \ \omega_l]^T \in \mathbb{R}^2$) is less than the number of degrees of freedom ($\xi_O \in \mathbb{R}^3$), imposed by the non-holonomic constrain $\dot{x}\sin\theta - \dot{y}\cos\theta = 0$.

B. Chassis Dynamic Model

The nonlinear relationship between the forces from each wheel on X_R direction (F_{xr}, F_{xl}) and the angular velocities ($\dot{\omega}_r, \dot{\omega}_l$) are given by¹

$$\begin{aligned} F_{xr} &= \left(\frac{M}{4} + \frac{I + Mh^2}{b^2}\right) r\dot{\omega}_r + \left(\frac{M}{4} - \frac{I + Mh^2}{b^2}\right) r\dot{\omega}_l + \\ &\quad + \frac{Mh}{b^2} r^2 (\omega_l^2 - \omega_r \omega_l), \\ F_{xl} &= \left(\frac{M}{4} - \frac{I + Mh^2}{b^2}\right) r\dot{\omega}_r + \left(\frac{M}{4} + \frac{I + Mh^2}{b^2}\right) r\dot{\omega}_l + \\ &\quad + \frac{Mh}{b^2} r^2 (\omega_r^2 - \omega_r \omega_l), \end{aligned} \quad (4)$$

where M and I are the chassis mass and the moment of inertia respectively, and b is the distance between the chassis center of mass and the reference point R .

C. DC Motor Dynamic Model

The DC motor model is presented as block diagram on the Figure 2, where s is the Laplace transform operator. The armature resistance R_a and inductance L_a , as well as the shaft moment of inertia J_m and damping coefficient b_m are constants in time. The electromechanical conversion is given by the constants $K_t = T_m/i_a$ and $K_e = e/\dot{\theta}_m$. Furthermore, armature current saturation, motor start dead zone and frictions (*Stiction* and *Coulomb*) are added as nonlinearities [20].

D. The Complete Robot Dynamic Model

Let a linear gear relationship between motor and wheel shafts given by $1/N$. It gives the relationships $\omega_m = N\omega$ and $F_r = N\tau$. Let also consider the same motor and wheel in both sides.

The dynamic relationships given by Equation 4 as well as the transfer function related with the block diagram in the Figure 2 yield the complete mobile robot model, given by the following equations² [15]:

$$\begin{aligned} J_r \dot{\omega}_{mr} &= \frac{K_t}{L_a s + R_a} u_r + \frac{K_t K_e}{L_a s + R_a} \omega_{mr} - \\ &\quad - \frac{r^2}{N^2} \left(\frac{M}{4} + \frac{I + Mh^2}{b^2} \right) \dot{\omega}_{mr} \\ &\quad - \frac{r^2}{N^2} \left(\frac{M}{4} - \frac{I + Mh^2}{b^2} \right) \dot{\omega}_{ml} - \\ &\quad - \frac{Mhr^3}{b^2 N^3} (\omega_{ml}^2 - \omega_{mr} \omega_{ml}) - b_m \omega_{mr} - \tau_{cr} \text{sign}(\omega_{mr}) - T_{sr}, \end{aligned} \quad (5)$$

$$\begin{aligned} J_l \dot{\omega}_{ml} &= \frac{K_t}{L_a s + R_a} u_l + \frac{K_t K_e}{L_a s + R_a} \omega_{ml} - \\ &\quad - \frac{r^2}{N^2} \left(\frac{M}{4} - \frac{I + Mh^2}{b^2} \right) \dot{\omega}_{mr} \\ &\quad - \frac{r^2}{N^2} \left(\frac{M}{4} + \frac{I + Mh^2}{b^2} \right) \dot{\omega}_{ml} - \\ &\quad - \frac{Mhr^3}{b^2 N^3} (\omega_{ml}^2 - \omega_{mr} \omega_{ml}) - b_m \omega_{ml} - \tau_{cl} \text{sign}(\omega_{ml}) - T_{sl}. \end{aligned} \quad (6)$$

III. THE CONTROL SYSTEM

A. Input-Output Feedback Linearization

The feedback linearization approach [21] is based on the cancelling of system nonlinearities while imposing desired linear dynamics. The central idea is to algebraically transform nonlinear system dynamics into fully or partly linear ones, so that linear control techniques might be applied.

Let a system described by the *companion form* as $\dot{x}^{(n)} = f_1(x) + f_2(x)u$, where $u \in \mathbb{R}^p$ is the control input, $x \in \mathbb{R}^n$ is the state vector and $f_1(x)$ and $f_2(x)$ are nonlinear function of states. Using the control input

$$u = (f_2)^{-1} [v - f_1], \quad (7)$$

and if f_2 is not singular the nonlinearities can be cancelled, hence an input-output relation $x^{(n)} = v$ is obtained. The control law v must be chosen such that the internal dynamics becomes stable. This approach has been efficiently applied for WMR motion control, see for example [16]–[18], [22].

B. The Follow the Carrot scheme

The *Follow the Carrot* [2], [5] trajectory tracking approach originates from the idea of holding a carrot in front of a horse to force the animal to move in desired direction.

Let $C_p = (x_{ref}, y_{ref}) \in \{O\}$ as the coordinates of the Carrot Point moving in a predefined time parametrized and obstacle free geometric path. The vector v_{cp} represents the Carrot Point velocity in the plane.

¹Complete details about this formulation, see [15].

²Due to may be possible to easily write these equations algebraically, the current saturation and the dead zone were neglected.

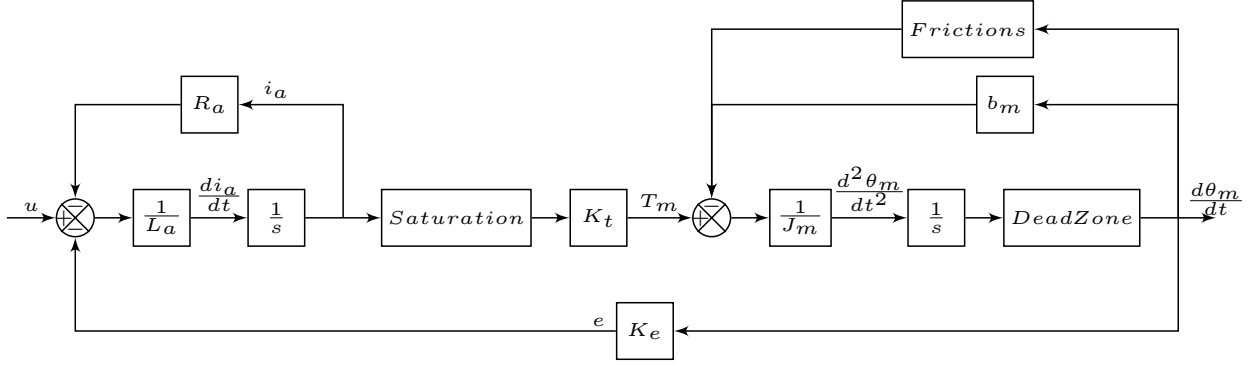


Fig. 2. Nonlinear DC motor model block diagram (adapted from [15]).

A virtual segment line is drawn from the center $R = (x, y) \in \{O\}$ of the robot to the Carrot Point C_p . Also a distance gap ρ within the same virtual segment line is considered to avoid singularity problems.

In face of these considerations, two errors are here defined: the linear error e_l , distance from the robot to the Carrot Point C_p ; and the heading error e_θ , the angle between the robot direction and the Carrot Point C_p , as illustrated by the Figure 3.

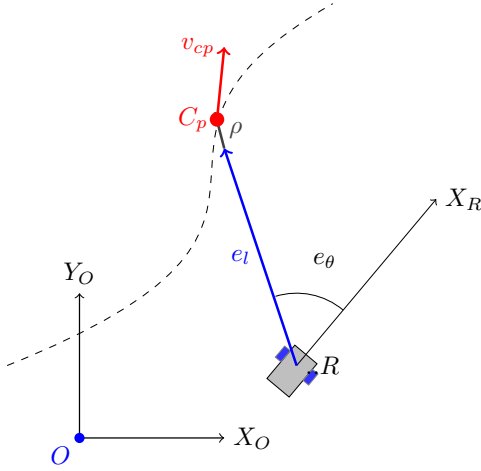


Fig. 3. The Follow the Carrot scheme.

The components of the linear error in the X_O and the Y_O directions are respectively given by $e_x = (x_{ref} - x)$ and $e_y = (y_{ref} - y)$. This way, the errors e_l and e_θ can be written as:

$$\begin{aligned} e_l &= \sqrt{e_x^2 + e_y^2} - \rho, \\ e_\theta &= \tan^{-1} \left(\frac{e_y}{e_x} \right) - \theta, \end{aligned} \quad (8)$$

and the error derivatives become

$$\begin{aligned} \dot{e}_l &= \frac{e_x(\dot{x}_{ref} - \dot{x}) + e_y(\dot{y}_{ref} - \dot{y})}{e_l}, \\ \dot{e}_\theta &= \frac{e_x(\dot{y}_{ref} - \dot{y}) - e_y(\dot{x}_{ref} - \dot{x})}{e_l^2} - \dot{\theta}. \end{aligned} \quad (9)$$

Substituting the kinematic unicycle model given by the Equation 3 (considering the angular wheel velocities as references, i.e., $\omega \rightarrow \omega_{ref}$) into the Equation 9 and after some algebraic manipulations yields

$$\begin{bmatrix} \dot{e}_l \\ \dot{e}_\theta \end{bmatrix} = f_{1R} \begin{bmatrix} \dot{x}_{ref} \\ \dot{y}_{ref} \end{bmatrix} + f_2 \begin{bmatrix} \omega_{refr} \\ \omega_{refl} \end{bmatrix}, \quad (10)$$

where the nonlinear functions of errors are

$$\begin{aligned} f_{1R} &= \begin{bmatrix} + \left(\frac{e_x}{e_l} \right) & + \left(\frac{e_y}{e_l} \right) \\ - \left(\frac{e_y}{e_l^2} \right) & + \left(\frac{e_x}{e_l^2} \right) \end{bmatrix}, \\ f_2 &= \begin{bmatrix} -\mathfrak{A} & -\mathfrak{A} \\ -\mathfrak{B} - \frac{r}{b} & -\mathfrak{B} + \frac{r}{b} \end{bmatrix}, \end{aligned} \quad (11)$$

with terms inside the f_2 matrix are given by:

$$\begin{aligned} \mathfrak{A} &= \left[\frac{r}{2e_l} (e_x \cos \theta + e_y \sin \theta) \right], \\ \mathfrak{B} &= \left[\frac{r}{2e_l^2} (e_x \sin \theta - e_y \cos \theta) \right]. \end{aligned} \quad (12)$$

Let choose the control signal:

$$\begin{bmatrix} \omega_{refr} \\ \omega_{refl} \end{bmatrix} = f_2^{-1} \cdot \left(K \begin{bmatrix} e_l \\ e_\theta \end{bmatrix} - f_{1R} \begin{bmatrix} \dot{x}_{ref} \\ \dot{y}_{ref} \end{bmatrix} \right), \quad (13)$$

where $K = \begin{pmatrix} K_l & 0 \\ 0 & K_\theta \end{pmatrix}$ is a diagonal matrix of gains. As algebraical canceling consequence, the dynamic of error become simply:

$$\begin{bmatrix} \dot{e}_l \\ \dot{e}_\theta \end{bmatrix} = K \begin{bmatrix} e_l \\ e_\theta \end{bmatrix} \quad (14)$$

The errors e_l and e_θ converge to zero if and only if the eigenvalues of K are negative.

C. Computational implementation

Both kinematic (Eq. 3) and dynamic model (Eq. 5 , 6) are implemented as Simulink systems. The error calculation (Eq. 8) and the pose controller (Eq. 13) are implemented as algorithms in Matlab environment. Furthermore, a PID algorithm is implemented in Matlab to handle with the robot dynamics and it controls the velocity of the robot wheels, named Velocity Controller. The aim of this controller is to bring the robot wheels velocities ω_r and ω_l to the references given by the equations 13.

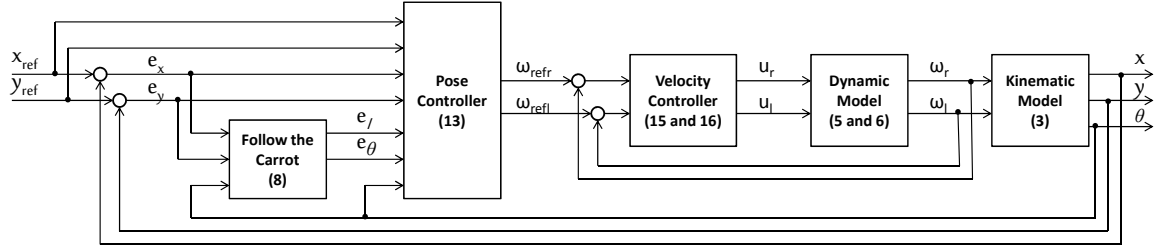


Fig. 4. Closed loop system block diagram. The numbers inside the blocks refer to the reference numbers of equations.

Due to implement a PID control law in terms of discrete time, the *velocity* (or *difference*) PID form is required. Let define the velocity errors $e_{\omega l} = (\omega_{refl} - \omega_l)$ and $e_{\omega r} = (\omega_{refr} - \omega_r)$, the velocity control signals at each time interval k are recursively given by:

$$\begin{aligned} du_r(k) &= (Kp_u + Ki_u + Kd_u)e_{\omega r}(k) - \\ &\quad - (Kp_u + 2Kd_u)e_{\omega r}(k-1) + (Kd_u)e_{\omega r}(k-2), \\ du_l(k) &= (Kp_u + Ki_u + Kd_u)e_{\omega l}(k) - \\ &\quad - (Kp_u + 2Kd_u)e_{\omega l}(k-1) + (Kd_u)e_{\omega l}(k-2). \end{aligned} \quad (15)$$

The subscript u refers to voltage; Kp_u , Ki_u , Kd_u are the PID gains. As result, the control signal are:

$$\begin{aligned} u_l(k) &= u_l(k-1) + du_l(k), \\ u_r(k) &= u_r(k-1) + du_r(k). \end{aligned} \quad (16)$$

This controller imposes the input voltages to the dynamic model which, in turns, gives to kinematic model the wheels angular velocities. The complete closed loop control system is illustrated as a block diagram in Figure 4.

IV. EXPERIMENTAL RESULTS AND DISCUSSIONS

The WMR motor and chassis parameters were chosen from an author real project. They are shown on Table I. All of the simulations were performed with time discretization $\delta t = 0.05s$.

TABLE I
THE WMR PARAMETERS

Motor			Geometry		
L_a	$6.2 \cdot 10^{-3}$	H	b	0.3	m
R_a	8.33	Ω	l	0.5	m
Ke	$3.95 \cdot 10^{-2}$	Vs/rad	d_f	0.15	m
Kt	$3.95 \cdot 10^{-2}$	Nm/A	r	0.1	m
bm	$8.13 \cdot 10^{-6}$	Nms/rad	h	0.0	m
J_m	$7.13 \cdot 10^{-9}$	kgm^2	M	10.0	kg
τ_c	$3.53 \cdot 10^{-3}$	Nms/rad	I	0.28	kgm^2
T_s	$7.80 \cdot 10^{-3}$	Nms/rad	N	19.7	rad/rad

Some sets of PID parameters were tested to choose empirically the optimal tuning via Ziegler and Nichols approach. The optimal set chosen is $[Kp_u, Ki_u, Kd_u] = [60.0, 10.0, 0.0]$.

Thereafter, with the gain matrix tuned as $K = \begin{pmatrix} -40 & 0 \\ 0 & -60 \end{pmatrix}$, and a gap $\rho = 0.1m$, some trajectories are tested as illustrated in Figure 5: a straight line and a circular pattern, both with constant velocity; a sinusoidal pattern with velocity component in the y direction constant and a spiral trajectory with exponential velocity. In all performed simulations, the WMR motion reaches predefined geometrical paths and tracks the reference which is defined by the movement of the Carrot Point C_P .

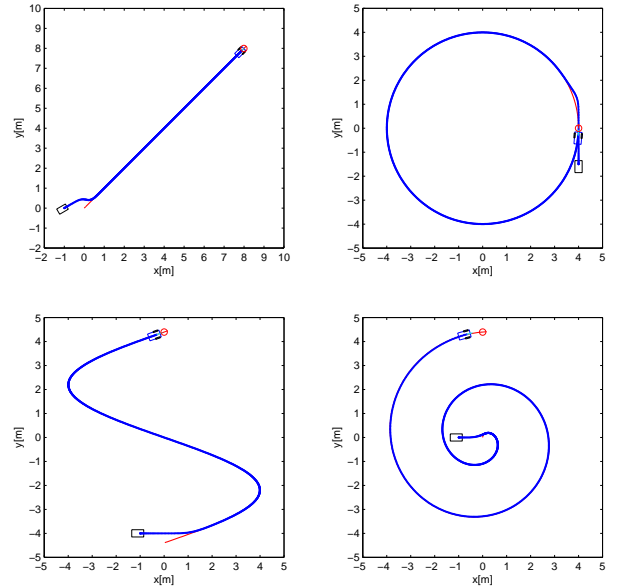


Fig. 5. Tested trajectories. The red line represents the desired geometric path and the blue line represents the WMR motion behavior.

Furthermore, a specific trajectory, with smooth and sharp curvature sections, is chosen in order to foster discussions about the effectiveness of this approach. The trajectory tracking simulation results are illustrated in Figure 6. Likewise, it is possible to note that after some transient period the geometric path is tracked satisfactorily.

The Figure 7 illustrated the relevant signals of this simulation. When the curve becomes a little sharper, on time instants $t = 5$, $t = 15$, $t = 25$ and $t = 35$, the controller acts to reject the disturbances and to stabilize the tracking task.

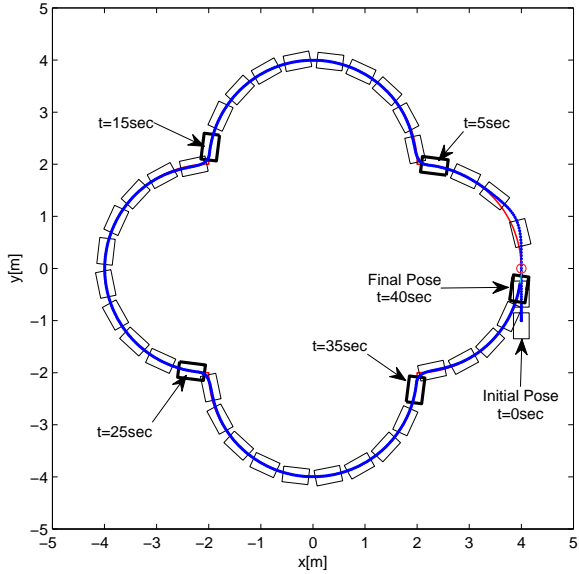


Fig. 6. The specific trajectory with a mix of curvature sections. Selected gains are $K_l = -40$ and $K_\theta = -60$.

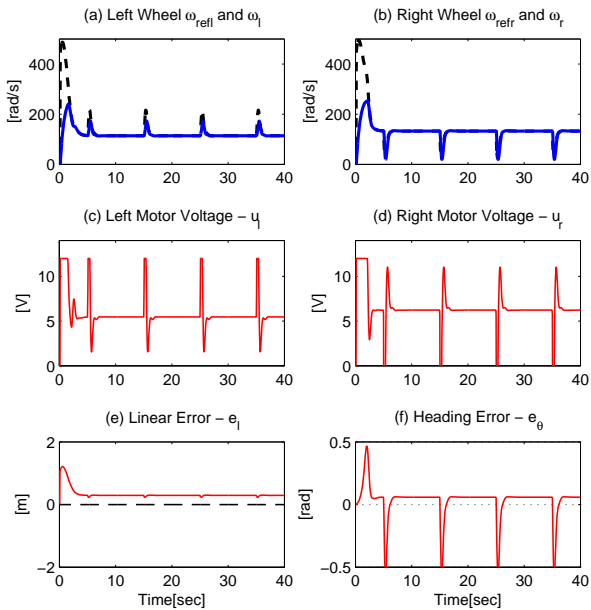


Fig. 7. The experiment signals: The left (a) and the right (b) angular wheel velocities and their references; the left (c) and the right (d) motor voltages; (e) the linear error and (f) the heading error.

In the bottom part of figure, it can be note that both the linear error e_l and the heading error e_θ do not converge to zero.

Finally, another extra experiment was performed to verify this steady state error in the long term behavior. An eight full cycle *lemniscata* trajectory was applied as reference for

360 seconds. In the same way, the gain matrix was tuned as $K = \begin{pmatrix} -40 & 0 \\ 0 & -60 \end{pmatrix}$. This simulation result can be viewed in the Figure 8.

The simulation error through the 360 seconds is illustrated in the Figure 9. It can be noted in both figures that even though the error is present, the WMR tracks the trajectory.

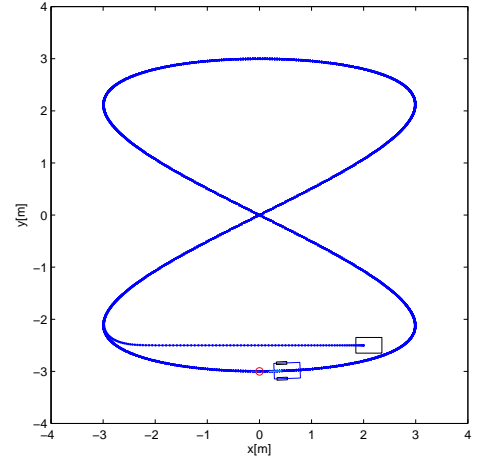


Fig. 8. An eight cycle lemniscata as reference to the WMR motion in red line, completely covered by the robot behavior in blue line.

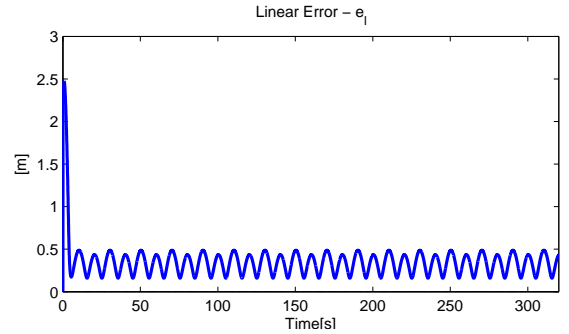


Fig. 9. The Linear Error e_l during the eight cycle lemniscata trajectory tracking.

V. CONCLUSIONS

In this paper, we have studied the trajectory tracking problem of a non-holonomic and highly nonlinear wheeled mobile robot model. The dual loop controller proposed contains a velocity PID controller and a novel input-output feedback linearization of the *Follow the Carrot* approach, as the work main contribution. Some simulations demonstrated that our proposed controller drives the WMR satisfactorily even in abrupt changes of the trajectory. Our future work is related to apply this controller to track trajectories generated by a real time planner.

REFERENCES

- [1] P. Svec, A. Thakur, E. Raboin, B. C. Shah, and S. K. Gupta, Target following with motion prediction for unmanned surface vehicle operating in cluttered environments, *Autonomous Robots*, vol. 36, no. 4, pp. 383–405, Nov. 2014.
- [2] M. Barton, Controller development and implementation for path planning and following in an autonomous urban vehicle, Thesis, University of Sydney, 2001.
- [3] R. C. Coulter, Implementation of the pure pursuit path tracking algorithm, Robotics Institute, Pittsburgh, PA, Tech. Rep. CMU-RITR-92-01, January 1992.
- [4] R. Hogg, A. Rankin, S. Roumeliotis, M. McHenry, D. Helmick, C. Bergh, and L. Matthies, Algorithms and sensors for small robot path following, in *IEEE International Conference on Robotics and Automation*, vol. 4. Ieee, 2002, pp. 3850–3857.
- [5] P. Sujit, S. Saripalli, and J. Sousa, An evaluation of UAV path following algorithms, *European Control Conference*, no. 1, pp. 3332–3337, 2013.
- [6] T. Hellstrom and O. Ringdahl, Follow the Past: a path-tracking algorithm for autonomous vehicles, *International Journal of Vehicle Autonomous Systems*, vol. 4, no. 2-4, pp. 216–224, 2006.
- [7] J. Wit, C. D. Crane, and D. Armstrong, Autonomous ground vehicle path tracking, *Journal of Robotic Systems*, vol. 21, no. 8, pp. 439–449, Aug. 2004.
- [8] T. Yeu, S. Park, and S. Hong, Path tracking using vector pursuit algorithm for tracked vehicles driving on the soft cohesive soil, in *SICE-ICASE*, 2006, pp. 2781–2786.
- [9] J. Bohren, T. Foote, and J. Keller, Little Ben: The Ben Franklin racing team’s entry in the 2007 Darpa urban challenge, *Journal of Field Robotics*, vol. 25, no. 9, pp. 598–614, 2008.
- [10] D. Aneesh, Tracking Controller of mobile robot, in *International Conference on Computing, Electronics and Electrical Technologies*, no. 4, 2012.
- [11] P. Encarnação and A. Pascoal, Combined trajectory tracking and path following control for dynamic wheeled mobile robots, in *IFAC World Congress*, 2002.
- [12] A. Aguiar and J. Hespanha, Trajectory-tracking and path-following of underactuated autonomous vehicles with parametric modeling uncertainty, vol. 52, no. 8, pp. 1362–1379, 2007.
- [13] X. Xiang, L. Lapiere, C. Liu, and B. Jouvencel, Path tracking: Combined path following and trajectory tracking for autonomous underwater vehicles, in *IEEE/RSJ International Conference on Intelligent Robots and Systems*. Ieee, Sep. 2011, pp. 3558–3563.
- [14] A. Alessandretti, A. Aguiar, and C. N. Jones, Trajectory-tracking and path-following controllers for constrained underactuated vehicles using Model Predictive Control, in *European Control Conference*, 2013, pp. 1371–1376.
- [15] M. Nørsgaard, N. Poulsen, and O. Ravn, Models for Iau’s Autonomous Guided Vehicle, Dept. of Mathematical Modelling - Technical University of Denmark, Lyngby, Tech. Rep., 2000.
- [16] D.-H. Kim and J.-H. Oh, Tracking control of a two-wheeled mobile robot using input–output linearization, *Control Engineering Practice*, vol. 7, no. 3, pp. 369–373, Mar. 1999.
- [17] G. Oriolo, a. De Luca, and M. Vendittelli, WMR control via dynamic feedback linearization: design, implementation, and experimental validation, *IEEE Transactions on Control Systems Technology*, vol. 10, no. 6, pp. 835–852, Nov. 2002.
- [18] D. Chwa, Tracking Control of Differential-Drive Wheeled Mobile Robots Using a Backstepping-Like Feedback Linearization, *IEEE Transactions on Systems, Man, and Cybernetics - Part A: Systems and Humans*, vol. 40, no. 6, pp. 1285–1295, Nov. 2010.
- [19] O. Akbati and G. Cansever, Control of pattern tracking nonholonomic mobile robot with feedback linearization, *IEEE International Conference on Electrical and Electronics Engineering*, no. 2, pp. 512–515, 2013.
- [20] B. Armstrong-Hélouvry, P. Dupont, and C. C. De Wit, A survey of models, analysis tools and compensation methods for the control of machines with friction, *Automatica*, vol. 30, no. 7, pp. 1083–1138, Jul. 1994.
- [21] J. Slotine and W. Li, *Applied nonlinear control*. Englewood Cliffs: Prentice-Hall, 1991.
- [22] B. D’Andrea-Novet, G. Bastin, and G. Campion, Dynamic feedback linearization of nonholonomic wheeled mobile robots,” in *IEEE International Conference on Robotics and Automation*, 1992, pp. 2527–2532.